

Selective Spreading and Jetting of Electrically Driven Dielectric Films

Pilnam Kim,¹ Camille Duprat,¹ Scott S. H. Tsai,² and Howard A. Stone^{1,*}

¹*Department of Mechanical and Aerospace Engineering, Princeton University, Princeton, New Jersey 08544, USA*

²*School of Engineering and Applied Sciences, Harvard University, Cambridge, Massachusetts 02138, USA*

(Received 14 March 2011; published 12 July 2011)

We study the electrically driven spreading of dielectric liquid films in wedge-shaped gaps across which a potential difference is applied. Our experiments are in a little-studied regime where, throughout the dynamics, the electrical relaxation time is long compared to the time for charge to be convected by the fluid motion. We observe that at a critical normal electric field the hump-shaped leading edge undergoes an instability in the form of a single Taylor cone and periodic jetting ensues, after which traveling waves occur along the trailing thin film. We propose a convection-dominated mechanism for charge transport to describe the observed dynamics and rationalize the viscosity dependence of the self-excited dynamics.

DOI: 10.1103/PhysRevLett.107.034502

PACS numbers: 47.65.-d, 68.15.+e

Electric fields offer a means to manipulate liquids over a wide range of length scales, which leads to various applications, including ink-jet printing [1], electrospray ionization for use in mass spectrometry [2], electrowetting [3], fluid mixing [4], patterning of thin polymer films [5] and control of microscale or nanoscale droplets [6]. Moreover, the electrically driven motion of fluids, i.e., electrohydrodynamics (EHD), gives rise to fundamental questions, such as the development of singularities [7] or the noncoalescence of oppositely charged drops [8]. One way to characterize EHD motions is to distinguish cavity flows driven by tangential electric stresses [9,10], instabilities of planar interfaces driven by normal electric stresses [11,12], and electrojetting, which typically combines both the influence of normal and tangential electric stresses [13,14]. In the absence of a separate pumping mechanism, electric fields can be used to manipulate liquids in confined geometries. Here we study such dynamics for manipulating thin liquid films, identify features of the flow that are self-regulated due to tangential and normal components of the field, and illustrate how this problem combines flow and instability found in other distinct EHD phenomena.

The EHD motion of thin liquid films, of typical thickness h , depends on the electrical properties of the fluid, i.e., the conductivity σ and dielectric constant ϵ , as well as the viscosity μ . The physical response involves the charge relaxation time t_e as well as the time t_c to rearrange or convect the liquid. The former is defined as the ratio of permittivity $\epsilon\epsilon_0$ (where the vacuum permittivity is $\epsilon_0 = 8.85 \times 10^{-12}$ F/m) and conductivity of the fluid, i.e., $t_e = \epsilon\epsilon_0/\sigma$. The latter is given by $t_c = h/u$, where u is the average speed of a viscous flow driven by a pressure difference $\Delta p \propto \epsilon\epsilon_0 E^2$ owing to Maxwell stresses, on the typical distance h , i.e., $\mu u/h \approx \Delta p$ or $t_c = \mu/\epsilon\epsilon_0 E^2$, where E is the magnitude of the electric field and μ is the fluid viscosity. The ratio of these two time scales defines an electric Reynolds number, $\mathcal{R}_{el} = t_e/t_c = \epsilon^2 \epsilon_0^2 E^2 / \mu \sigma$ [15]. The complete characterization of this

type of free surface flow problem requires an additional dimensionless parameter that compares viscous effects to inertia and surface tension, i.e., the Ohnesorge number $Oh = \mu/(\rho\gamma h)^{1/2}$, where γ and ρ are the surface tension and density, respectively.

The majority of EHD studies in the literature [16–20], with the exception of unstable jetting observed in silicone oils [21], are characterized by a small value of \mathcal{R}_{el} ($\ll 1$), that is, charges are transported by Ohmic conduction because the charge relaxation time t_e is always the shortest time scale in the system. Nevertheless, in studies of jetting driven by electrical stresses, where a liquid jet emanates from a conical meniscus, the hydrodynamic time t_c is locally shorter than the charge relaxation time scale due to rapid fluid motion at the cone-jet transition, even for high conductivity liquids [14,16]. Between jetting events, charges may rearrange quickly due to a short electrical relaxation time scale. When the electrical conductivity is decreased so that $\mathcal{R}_{el} \gg 1$, t_c is the shortest time scale in the system for all dynamical processes; charge transport is then dominated by convection processes only, which suggests a fundamental change in the EHD motions. This subject is the focus of our Letter.

To explore the dynamics when $\mathcal{R}_{el} \gg 1$, we consider the electrically driven spreading of a dielectric liquid film below an inclined planar PET (polyester) electrode with width w and inclination angles $1.9^\circ \leq \alpha \leq 4.9^\circ$ [Fig. 1(a)]. We use silicone oils with viscosities $4.6 \times 10^{-3} \leq \mu \leq 970 \times 10^{-3}$ Pa · s, density $\rho \approx 960$ kg/m³, surface tension $\gamma \approx 20 \times 10^{-3}$ N/m, conductivity $\sigma \approx 10^{-13}$ S/m, and dielectric constant $\epsilon \approx 2.5$; the low conductivity of the silicone oil is due to a small amount of free charge that results from unavoidable contamination during processing. The electrode is electrified by rubbing it with a piece of paper to obtain a negatively charged surface with a uniform potential ϕ_0 , which can vary up to 3 kV as measured by a surface dc volt meter (AlphaLab, Inc.). A dielectric liquid film of initial thickness h_0 is placed on a

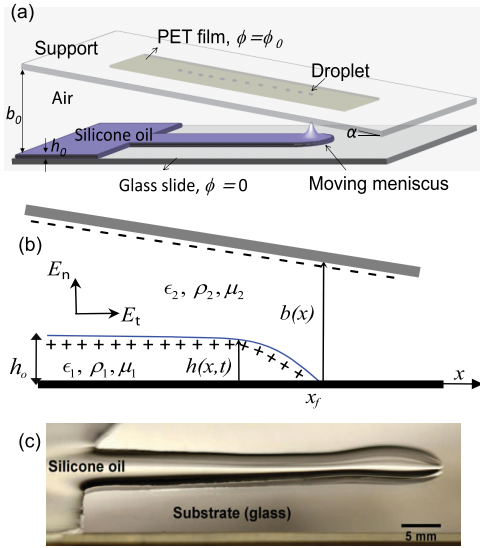


FIG. 1 (color online). (a) Schematic diagram of the experimental setup. (b) Side view of the system. The (+) and (-) signs represent the positive and negative free charges. (c) Final shape of the selectively spread liquid film, which has the shape of the applied rectangular electrode.

grounded glass substrate ($\epsilon_g \approx 6.7$) in direct contact with an aluminum plate ($\epsilon_{Al} \approx 10$) at potential $\phi = 0$. The equilibrium contact angle of silicone oil with the glass substrate is $\theta_{eq} \approx 10^\circ$ and the initial gap b_0 between the substrate and the PET film is varied, $5 \text{ mm} \leq b_0 \leq 6.2 \text{ mm}$ [Fig. 1(b)]. Gravitational effects are not expected to be significant, since the initial thickness of the liquid film is approximately $300 \text{ }\mu\text{m}$, which is small compared to the capillary length, $\ell_c = \sqrt{\gamma/\rho g} = 1.5 \text{ mm}$ for silicone oil, where g is the acceleration due to gravity. Furthermore, the Ohnesorge number is mostly of order unity ($0.05 < Oh < 11$), which implies that viscous effect dominates over inertial and capillary effects.

The experimental system acts as a capacitor and, due to the inclined electrode, both normal and tangential electric fields (E_n and E_t) are generated in the gap. Thus, after being placed under the electrode, the liquid-air interface is charged due to the induced polarization associated with the capacitor, so that positive charges present in the liquid accumulate at the liquid-air interface [Fig. 1(b)]. The liquid moves from the reservoir and flows under the electrode toward the region of larger electric field, with speed significantly faster than that due to either gravity or capillarity. We denote the position of the electrode as $y = b(x)$, in which case the magnitude of the electric field acting on a given point of the interface $h(x, t)$ is given approximately by $E_n(x, t) \approx \phi_0/(b(x) - h(x, t))$, since most of the potential drop occurs across the air gap. Consequently, the liquid spreads as a strip that has the width and shape of the applied rectangular electrode [Fig. 1(c)], which highlights this approach for selectively manipulating dielectric liquids.

A typical example of the spreading motion is shown with the sequence of photographs in Fig. 2 (see also the

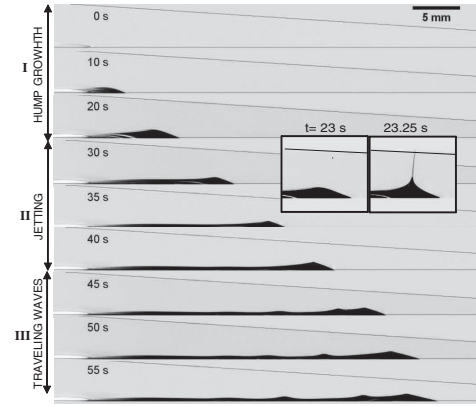


FIG. 2. Sequence of the side view of a thin film of silicone oil ($h_0 = 0.35 \text{ mm}$, $\mu = 19 \text{ mPa} \cdot \text{s}$) flowing under a rectangular electrode ($\phi_0 = 1200 \text{ V}$, $b(0) = 5.4 \text{ mm}$, $\alpha = 3.5^\circ$). Three different regimes are identified, which are denoted as (I) a growing hump at the front, (II) jets emitted from the tip of the hump (inset shows a typical jetting event), and (III) traveling waves.

supplementary movie [22]). We observe three successive regimes during film spreading, which we denote hump growth (I), jetting (II), and traveling waves (III). In the first regime, the film follows the inclined electrode, flows along the gap, and the initially flat interface deforms and grows a single asymmetric hump at the front. As the film moves under the inclined electrode, jetting occurs repeatedly from the tip of the hump (regime II, insets of Fig. 2). Thereafter, small amplitude waves appear along the liquid film, and travel toward the front (regime III). In these experiments, the electrical relaxation time is $t_e = \epsilon\epsilon_0/\sigma = 200 \text{ s}$, which is large compared to the convection time $t_c = \mu/\epsilon\epsilon_0 E_\infty^2 \approx 20 \text{ ms}$, and even long compared to the time ($\approx 55 \text{ s}$) of the spreading motion shown in Fig. 2. Next, we describe the physical origin of the three distinct regimes, and show that the observed EHD instabilities, i.e., the pulsating jets (regime II) and the traveling waves (regime III), are controlled by the shortest time scale for charge rearrangement, which here is $t_c \propto \mu$.

We first focus on regime I and the transition to regime II (hump-jet transition). The experimental profiles of the growing hump obtained for increasing times, increasing electric field E_n , are shown in Fig. 3(a). As the front moves, the gap between the electrode and the liquid interface decreases; i.e., the normal electric field increases. The interface is destabilized by electrical stresses: the hump grows, rapidly changes shape to exhibit a sharper tip, then a jet is emitted. After the onset of jetting, and even though the electric field is increasing, we observe that the height of the hump $h_{max}(t)$ is constant while the film continues to move along the gap and the hump emits a jet [Fig. 3(b), top] at regular time intervals. Thus, we identify that, when both normal and tangential components of the electric fields are present, this film flow is self-regulated, in that it establishes a constant height with periodic jetting. We track the position $x_f(t)$ of the liquid front and measure the spreading velocity $v_f(t)$ [Fig. 3(b), bottom]. We observe

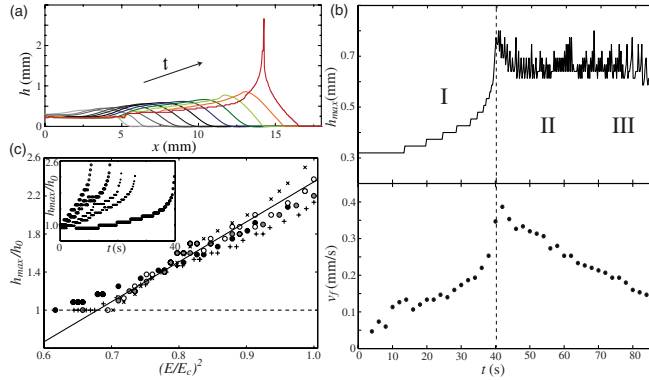


FIG. 3 (color online). (a) Time-dependent experimental shape profiles of the liquid film ($h_0 = 0.35$ mm, $\mu = 19$ mPa \cdot s) spreading under an electrode [$\phi_0 = 1200$ V, $b(0) = 5.4$ mm, $\alpha = 3.5^\circ$]. Time between successive profiles $\Delta t = 2.5$ s. (b) Corresponding temporal evolution of the hump height (top), the maximum thickness of the film $h_{\text{max}}(t)$, and spreading velocity v_f (bottom), as function of time. The vertical dashed line corresponds to the onset of tip jetting. Here we have not plotted the points corresponding to the jet touching the upper electrode [$h_{\text{max}} = b(x_{\text{max}})$]. (c) The evolution of the height of hump in regime I with increasing electric field. Inset: evolution of h_{max} as a function of time. The symbols represent data for $\alpha = 3.5^\circ$, $b_0 = 5.4$ mm and $\mu = 4.6$ mPa \cdot s (open circles), 9.3 mPa \cdot s (gray solid circles) and 19 mPa \cdot s (black solid circles); $\alpha = 3.5^\circ$, $b_0 = 6.2$ mm and $\mu = 19$ mPa \cdot s (+); $\alpha = 1.9^\circ$, $b_0 = 5.4$ mm and $\mu = 19$ mPa \cdot s (\times).

two different behaviors: the speed first increases as the hump grows (I), then the speed decreases until a quasisteady state is reached while jetting occurs (II). The maximum speed is at the transition between regimes I and II.

The rapid growth of the hump can be rationalized by measuring $h_{\text{max}}(t)$ as a function of the local normal electric field, $E_n(x_{\text{max}}, t)$ at the position of the maximum $x_{\text{max}}(t)$. All of our data for different liquid viscosities, inclination angles, and gap heights between the electrode and the film collapse onto a single curve. The height of the hump is proportional to E_n^2 , as expected [Fig. 3(c)]. There is no significant difference in the hump growth when the fluid viscosity is varied between 4.7–970 mPa \cdot s; the fluid viscosity only affects the average spreading speed [Fig. 3(c)].

The sharp hump-jet transition illustrated in Fig. 3(b) implies the existence of a critical electrical field E_c for the onset of the jetting instability. We measured the gap height at which the jet occurs for various viscosities, inclination angles α , and initial gaps b_0 . Once the hump reaches $b - h \approx 4$ mm, corresponding to a critical electric field $E_c \approx 3 \times 10^5$ V/m, the hump rapidly becomes unstable, subsequently deforms into a cusp shape, and a jet is emitted. We can understand the threshold value E_c by considering a balance of electric stress ($\epsilon\epsilon_0 E^2$) and capillary pressure ($2\gamma/r$), which gives

$$E_{n,c} \approx c_1 \left(\frac{2\gamma}{\epsilon\epsilon_0 r} \right)^{1/2}, \quad (1)$$

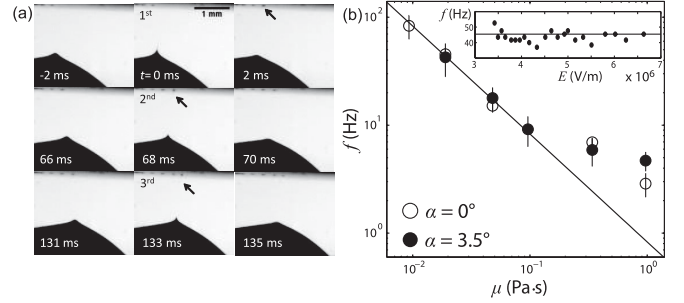


FIG. 4. (a) High-speed images of three successive jetting events ($\mu = 45$ mPa \cdot s). A cusp shape appears before the jetting, and a conical geometry of the hump is recovered after the jet is emitted. This hump-jet transition is repeated for three successive jets. (b) Jetting frequency f as a function of viscosity for a flat (open circles) and inclined (solid circles) electrode in regime II. The solid line corresponds to $f = c_2 \frac{2\gamma}{\mu r}$ with $c_2 = 0.83$.

where r is the radius of the hump (taken as $w/2$ since the width of the hump, w , sets the size of the advancing finger). The constant $c_1 \approx 0.32$ as estimated for a spherical liquid drop in air [23]. From (1), the estimated value $E_{n,c} \approx 2.85 \times 10^5$ V/m $\approx E_c$, which is in good agreement with the experiments. Furthermore, we verified that E_c is independent of the tangential electric field, as well as the viscosity of the liquid, as expected from Eq. (1).

The behavior of the pulsating jet in regime II is captured in the series of images shown in Fig. 4(a). We illustrate three successive jets at the hump-jet transition. The emitted droplets are deposited directly onto the surface of the electrode [black arrows in Fig. 4(a)]. From our observations, the shape of the hump persists throughout jetting, and local deformation in the form of a cusp shape is observed just before jetting.

Pulsating jets have been studied for conductive liquids under external control, including a pulsed voltage (ac electric field) or control of the liquid flow rate [24,25]. Such dynamics are accompanied by the retraction of the conical shape after jetting [26] and models of inertial dynamics are appropriate. In contrast, the jets observed in our experiments continue without complete retraction of the hump [Fig. 4(a)]. Moreover, in our system, the flow rate is intrinsically regulated by tangential stresses along the film and viscous effects. Also, the jetting time (< 2 ms) is significantly shorter than the time between successive jets (≈ 100 ms). In a quasisteady state, if some free charges are lost at the interface through the emission of a jet, the same amount of charge is convected from the bulk. Therefore charge transport, characterized by the convection time $t_c = \mu / \epsilon\epsilon_0 E_\infty^2$, regulates the periodic jetting.

To understand the underlying mechanism behind the pulsating jets reported here, we measure the average value of the jetting frequency f for various viscosities under a flat ($\alpha = 0^\circ$) or inclined ($\alpha = 3.5^\circ$) electrode for both moving and pinned contact lines [Fig. 4(b)]. The jetting frequency decreases linearly with increasing viscosity and

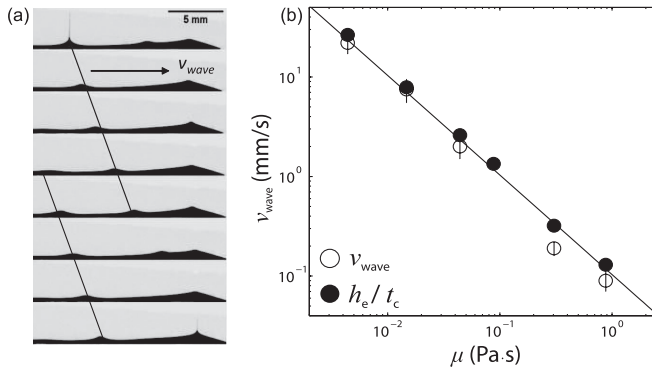


FIG. 5. (a) Image sequence of the liquid film in regime III. Time between successive images $\Delta t = 250$ ms. The humps that are evident have pulsating jets at their tips. The speed of the waves is nearly constant, as indicated by the straight lines that track the waves in the images, except when the wave approaches the front. (b) Wave velocity v_{wave} as a function of viscosity.

is independent of the electric field [inset in Fig. 4(b)]. The time between two successive jets is then given by the time taken by the charges to be convected to the tip of the hump, which has length scale $r \approx w/2$. The frequency can then be estimated by $f = \langle u \rangle / r$, where the average speed $\langle u \rangle$ is obtained from the viscous flow thin-film equation, i.e., $\langle u \rangle \approx r \Delta p / \mu$ with a typical pressure difference $\Delta p \approx \epsilon \epsilon_0 E_c^2 \approx 2\gamma / r$, i.e. $f \approx t_c^{-1}$ at the critical electric field E_c . Thus, we estimate the intrinsic frequency

$$f = c_2 \frac{2\gamma}{\mu r}. \quad (2)$$

This relation is verified experimentally with a fitting parameter $c_2 = 0.83$ [Fig. 4(b)]. According to (2), the jetting frequency can be tuned by varying the viscosity or the width of the electrode, and should be contrasted with other studies where the pulsation frequency is regulated by inertial effects (e.g., [26]).

We note that at late times in regime II, although most of the liquid is experiencing a normal electric field $E_n \gtrsim E_c$, only one hump is present and the thickness of the trailing liquid film is approximately constant $h(x, t) \approx h_e$. This observation of the undeformed film indicates that the tangential component of the electrostatic field E_t plays a crucial role in stabilizing the film. The effect of viscosity on the instabilities is also observed in the traveling wave regime (regime III). We provide a sequence of images that shows that two individual waves appear along the initially smooth interface and propagate at the same speed toward the hump at the front [Fig. 5(a)]. Once the waves appear, the front slows down and can even stop. Since we are in a viscous overdamped regime, the waves are only associated with the dynamics of the film rather than relaxation processes at the hump. We measured the speed of the waves, v_{wave} as a function of μ , and found that $v_{\text{wave}} \propto \mu^{-1}$ [Fig. 5(b)]. Since t_c is a critical time scale in the system, the wave velocity, according to the thin-film approximation,

can be estimated by $v_{\text{wave}} \approx h_e / t_c$, where h_e is the equilibrium thickness of the film ($\approx 200 \mu\text{m}$). The data collapse onto this predicted value (solid line).

Our findings highlight the significance of a viscosity controlled, convection-dominated mechanism for charge transport in the EHD motion of dielectric films and jets. The selective spreading and the periodic jetting following a moving front are features that may find use in other systems.

Funding for this work was provided by the NRF of Korea (NRF-2009-352-D00034) and the ARO MURI (W911NF-09-1-0476).

*hastone@princeton.edu

- [1] J.-U. Park *et al.*, *Nature Mater.* **6**, 782 (2007).
- [2] J. B. Fenn *et al.*, *Science* **246**, 64 (1989).
- [3] R. A. Hayes and B. J. Feenstra, *Nature (London)* **425**, 383 (2003).
- [4] A. O. El Moctar, N. Aubry, and J. Batton, *Lab Chip* **3**, 273 (2003).
- [5] E. Schaffer, T. Thurn-Albrecht, T. Russell, and U. Steiner, *Nature (London)* **403**, 874 (2000).
- [6] I. G. Loscertales *et al.*, *Science* **295**, 1695 (2002).
- [7] L. Oddershede and S. R. Nagel, *Phys. Rev. Lett.* **85**, 1234 (2000).
- [8] W. D. Ristenpart *et al.*, *Nature (London)* **461**, 377 (2009).
- [9] J. R. Melcher and G. I. Taylor, *Annu. Rev. Fluid Mech.* **1**, 111 (1969).
- [10] R. Raghavan *et al.*, *Sens. Actuators B Chem.* **140**, 287 (2009).
- [11] L. Tonks, *Phys. Rev.* **48**, 562 (1935).
- [12] G. I. Taylor and A. D. McEwan, *J. Fluid Mech.* **22**, 1 (1965).
- [13] A. Barrero *et al.*, *Phys. Rev. E* **58**, 7309 (1998).
- [14] R. T. Collins, J. J. Jones, M. T. Harris, and O. A. Basaran, *Nature Phys.* **4**, 149 (2008).
- [15] J. C. Baygents, N. J. Rivette, and H. A. Stone, *J. Fluid Mech.* **368**, 359 (1998).
- [16] J. F. De La Mora and I. G. Loscertales, *J. Fluid Mech.* **260**, 155 (1994).
- [17] D. A. Saville, *Annu. Rev. Fluid Mech.* **29**, 27 (1997).
- [18] P. Notz and O. Basaran, *J. Colloid Interface Sci.* **213**, 218 (1999).
- [19] A. M. Ganan-Calvo, *J. Fluid Mech.* **507**, 203 (2004).
- [20] J. Fernandez de la Mora, *Annu. Rev. Fluid Mech.* **39**, 217 (2007).
- [21] H. B. Zhang, M. J. Edirisinghe, and S. N. Jayasinghe, *J. Fluid Mech.* **558**, 103 (2006).
- [22] See Supplemental Material at <http://link.aps.org/supplemental/10.1103/PhysRevLett.107.034502> for a movie of a thin film of silicone oil flowing under a rectangular inclined electrode (as in Fig. 2).
- [23] G. I. Taylor, *Proc. R. Soc. A* **313**, 453 (1969).
- [24] C. H. Chen, D. A. Saville, and I. A. Aksay, *Appl. Phys. Lett.* **89**, 124103 (2006).
- [25] H. K. Choi *et al.*, *Appl. Phys. Lett.* **92**, 123109 (2008).
- [26] I. Marginean, L. Parvin, L. Heffernan, and A. Vertes, *Anal. Chem.* **76**, 4202 (2004).